14 Micro Energy and Chemical Systems (MECS) and Multiscale Fabrication

B. K. Paul

Nano/Micro Fabrication Facility, Oregon State University

14.1 Introduction

Over the past 40 years, there has been a large and growing emphasis on the fabrication of devices with ever-decreasing dimensions spread over multiple length scales. These so-called multiscale systems are here defined as integrated systems with sub-millimeter features spanning more than three orders of magnitude. One example of a multiscale system is the integrated circuit (IC) where feature sizes may range four or more orders of magnitude from 100 nanometer gates to millimeter-scale bonding pads. The drive toward multiscale systems is obvious. On one end, smaller gate sizes permit higher component densities improving both speed and cost. At the other end, macro-scale pads are required for electrical interconnection with the macro-world. As shown in Table 14.1, other examples of multiscale systems involve mechanical miniaturisation including microelectromechanical systems (MEMS), micro total analysis systems (μTAS) and micro energy and chemical systems (MECS).

Over three decades ago, mechanical miniaturisation was introduced through pioneering biomedical research at Stanford (Samaun et al. 1973; Middlehoek et al. 1980). Since then, many applications have been developed such as automotive accelerometers, inkjet printers, microelectronics cooling, point-of-use chemical synthesis, and man-portable power generation to name a few. MEMS were the first of these devices to develop. MEMS are highly miniaturised electromechanical devices used for microscale energy conversion (transduction). Typical applications are as miniature sensors and actuators such as accelerometers for automotive air bags, thermal inkjet printheads, micromirror arrays for computer projection and read/write magnetic memory heads. Typical feature sizes are on the order of one to ten μm. MEMS technology enables highly complex assemblies without the need for mechanical assembly. The basis of MEMS fabrication is integrated circuit (IC) processing and silicon micromachining techniques. The traditional manufacturing engineering community did not

contribute much to the process development necessary to enable ICs and MEMS. This was in part due to the fact that the science base needed to manipulate matter for the processing of electrons is fundamentally different than the manufacturing science for producing structural systems. Then to, the precision in ICs and MEMS were at levels previously unattainable in traditional manufacturing. Feature sizes in these systems were on or below the order of traditional manufacturing tolerances. Whole new fields of dimensional and compositional analysis were required. Finally, in traditional manufacturing, systems integration across multiple length scales was provided mainly through mechanical assembly, which could be managed by unskilled laborers. Consider the mechanical assembly of airplanes or automobiles, which could involve hundreds or thousands of workers in contrast with automated IC integration. Consequently, manufacturing engineers did not perceive their skill set to be applicable at the small scale.

Table 14.1. Different types of miniaturisation in use today

Parameter	ICs	MEMS	μTAS	MECS
Function	Signal processing	Signal acquisition	Lab-on-chip	Process intensification
Primary materials	Semiconductor	Silicon	Silicon, glass and polymer	Metal, ceramics and polymers
Key elements	Transistors	Transducers	μFluidic pumps and valves	μChannel arrays
Feature size	100 nm	μm	Tens of μm	25 to 250 μm
System size	mm to cm	mm to cm	mm to cm	Mm to meters

However, new microfluidic technologies are beginning to emerge providing the manufacturing engineer an opportunity to participate in the multiscale revolution. μTAS (also known as BioMEMS) are microfluidic systems used for chemical, biological or biochemical manipulation and analysis. These microfluidic devices may incorporate many of the transduction concepts from ICs and MEMS into microchannels or microwells to collect data and information based on assays performed on nanoliters or picoliters of fluid. A popular application of μTAS recently has been DNA analysis-on-a-chip which has contributed significantly to the decoding of the human genome (Weigl et al. 1999). Due to their ability to replace long, arduous chemical assaying procedures, μTAS systems are sometimes referred to as “lab-on-a-chip” technology. In constrast, MECS are microfluidic devices, which rely on highly-paralleled, embedded microchannels for the bulk processing of mass and energy. There are numerous advantages of microfluidic systems that are common to both μTAS and MECS. First of all, microfluidic devices all have high surface area to volume ratios, which shortens the diffusion

distances and provides high rates of heat and mass transfer. Secondly, certain conditions such as high pressures can generally be sustained in these systems, which are hard to sustain in macro-scale systems since, in the case of high pressures, the surface areas are reasonably small and the resultant forces are also small. Lastly, the functional parts of the systems all operate with small volumes of fluid. Consequently, these systems permit excellent temperature control with the ability to rapidly mix and quench materials. The major difference in μTAS and MECS technology is the volume of fluid processed. MECS devices are typically based on arrays of microchannels in order to handle much larger volumes of fluid and also typically have more demanding chemical and thermal property requirements. Consequently, the overall size of MECS devices ranges between a few millimeters for portable power systems to over one meter for distributed fuel reforming.

Fig. 14.1 shows a small slice of the current and future microfluidic applications that will benefit from nano and microtechnology integration. Already much of the biological revolution has benefited from the accelerated heat and mass transfer available within microchannels. Continued advances in lab-on-a-chip technology are fueling radical innovations in medicine. Similar microtechnology is beginning to show promise as a means for economically producing nanomaterials. Other multiscale trends are toward the decentralised processing of mass and energy. In the future, residential air conditioning will be made "ductless" through the application of many distributed micro heat pumps resulting in large energy savings. Microchannel reactors with nanostructured catalysts will make on-site waste cleanup a reality lending to the realisation of "green" manufacturing. Portable kidney dialysis based on multiscale technology will make life more manageable (and cost effective) for a whole new generation of kidney patients.

New fabrication approaches are being developed to advance these technologies. While material processing requirements for MEMS revolve around electromechanical integration leading to IC processing and silicon micromachining, material processing for μTAS generally involves polymer processing due to near ambient device operating conditions. However, many of the devices shown in Fig. 14.1 are MECS devices. Unlike MEMS and μTAS devices, MECS devices require highly-paralleled arrays of microchannels made from more traditional engineering materials. MECS devices are produced by a fabrication approach known as microlamination (Paul et al. 1999). Microlamination consists of the patterning and bonding of thin layers of material, called laminae, to generate monolithic devices with embedded microchannel features.

Within this context, a new role for the manufacturing engineer emerges as new methods for economical multiscale fabrication are investigated. Future challenges lie in the breadth of material and dimensional integration required. Compare the mechanical assembly of an airplane with wingspans on the order of tens of meters and electrical subassemblies on the order of millimeters (four orders of magnitude) with the integration of thermal electric generation (TEG) superlattices with resolution on the sub-nanometer scale into a portable power generator with overall system sizes approaching one meter (over nine orders of magnitude). New

multiscale fabrication methods emphasise fabrication, assembly and characterisation of more traditional engineering materials including metals, ceramics and selected polymers due to a need for different thermal and chemical properties. Advances in material science are needed to refine grain sizes and provide better compositional homogeneity at the small scale. Further, many of these monolithic, integrated systems are produced by shaping and joining discrete pieces of material – the domain of the manufacturing engineer.

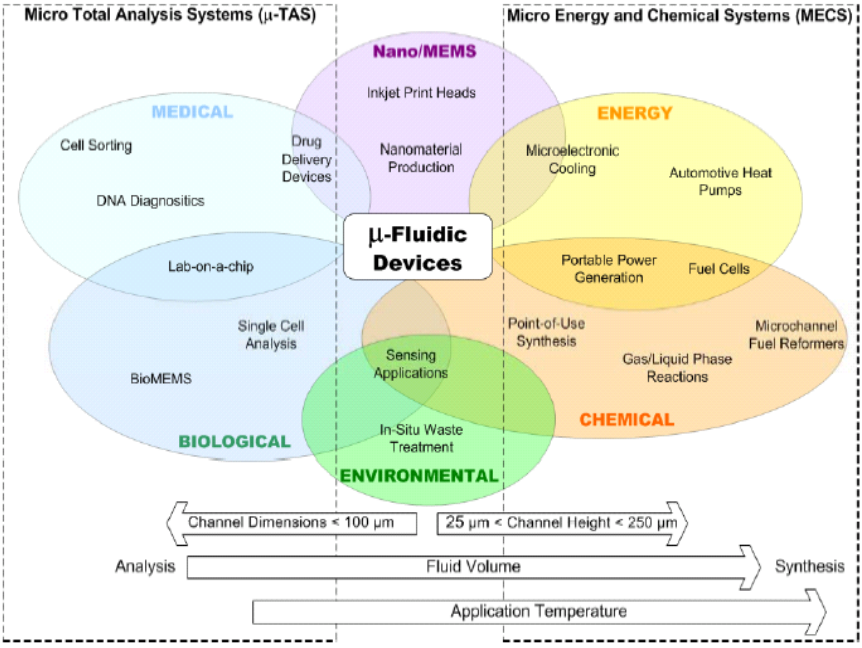

Fig. 14.1. Microfluidic applications-Multiscale fabrication (Courtesy: Pluess)

This chapter includes the findings from seven year's of study of microlamination processes conducted at the Oregon State University (OSU) Nano/Micro Fabrication (NMF) Facility. In sum, significant progress has been made toward understanding the source and effect of shape variation within microlaminated structures. Shape variation is defined as any change from the specification of the product's design such as rough surfaces, improper alignment or warpage. Other studies have been conducted to understand the economic drivers within microlamination processes. Also, new microlamination methods have been developed based on new material and geometry requirements. Future efforts are needed to overcome the economic and technological challenges of microlamination processes in order for MECS technology to become of substantial industrial and societal benefit. This chapter is organised into three sections. The first section provides a justification and foundation for microlamination and the current research being conducted in multiscale fabrication. The second section

consists of findings from specific investigations into technological issues within specific microlamination architectures. The final section explores the economics of MECS device fabrication via microlamination and provides implications for future research and development.

14.2 Micro Energy and Chemical Systems

The objective of this section is to lay the groundwork for a deeper discussion of MECS fabrication techniques. Specifically an overview of MECS is provided including a discussion of important MECS applications. An overview is given of some of the fabrication challenges associated with the large-scale production of MECS devices. The section concludes with an introduction to microlamination.

Micro Energy and Chemical Systems (MECS) are bulk microfluidic devices, which rely on embedded microstructures for their function. The overall size of MECS devices range between microscale systems, such as microelectromechanical systems (MEMS), and macroscale systems such as automobile engines and vacuum pumps. These mesoscopic systems are expected to provide a number of important functions where a premium is placed on either mobility, compactness, or point-of-use synthesis. The benefits of decentralised and portable energy and chemical systems are realised by the enhancement in heat and mass transfer performance within high surface-to-volume ratio microchannels. Other benefits of microchannels include rapid temperature changes, excellent temperature control, fast mixing, and the opportunity of operating at elevated pressures (Ameel et al. 1997, 2000; Peterson 2001). Implementations of MECS in heat transfer and chemical applications include microelectronic cooling systems (Kawano et al. 1998; Little 1990), chemical reactors (Martin et al. 1999; Matson et al. 1999), fuel processing (Daymo et al. 2000; Tonkovich et al. 1998), and heat pumps (Drost and Friedrich 1997; Drost et al. 1999, 2000) among others.

MECS devices are primarily focused on taking advantage of the extremely high rates of heat and mass transfer available in microscale geometries to radically reduce the size of a wide range of energy, chemical and biological systems. Typically a MECS device will have dimensions on the order of 1 to 10 cm but it will include embedded microscale geometries such as arrays of parallel microchannels where individual channel dimensions are on the order of 100 microns in width by several mm in height. By taking advantage of the enhanced rates of heat and mass transfer in the embedded microscale geometries, researchers have typically been able to reduce the size of a variety of energy and chemical systems by a factor of 5 to 10 (Brooks et al. 1999; Tonkovich et al. 1998; Warren et al. 1999). Typically MECS devices are fabricated in metals, ceramics or polymers and therefore cannot depend on conventional microfabrication techniques. Microlamination has proved to be an economical and flexible method for fabricating MECS devices (Porter et al. 2002). MECS devices are occasionally referred to as mesomachines and in Europe, research in this area is identified as process intensification.

14.2.1 Heat and Mass Transfer in MECS Devices

Typical MECS devices include individual microscale geometries with dimensions on the order of 100 microns. Single-phase flow in a 100-micron wide channel will in almost all cases of interest be laminar, with Reynolds numbers typically between 1 and 100. In laminar flow, the residence time required to have the fluid reach thermal equilibrium with the walls of the channel decreases as D^2 where D is the width of the channel. If we decrease the channel width by a factor of 10, we will decrease the required residence time by a factor of 100. A heat exchanger with 100 micron wide channels would be $1/100^{th}$ the size of a heat exchanger with 1 mm channels for the same heat transfer rate and it can be shown that for laminar flow, the increased pressure drop associated with the smaller channels is exactly offset by the decreased length of the channel required to deliver the same heat transfer rates. In effect we get a theoretical factor of 100 reduction in size with no increase in pressure drop. In practice microchannel heat exchangers have demonstrated heat fluxes 3 to 5 times higher than conventional heat exchangers. Ultimately, by going to smaller channels we will reduce the diffusion barrier to the point where other processes such as axial conduction along the heat exchanger determine residence time for thermal equilibrium. At that point, further reductions in channel dimensions will not result in reduced residence time. While single-phase flow in microchannels is well understood, processes that involve wall effects such as phase change and surface tension are significantly different in microscale geometries. Boiling is an example. The limited experimental investigations of boiling in microchannels suggest that the process of phase change in a microchannel is different from macro scale devices. However, published performance for microchannel evaporators and condensers show a significant improvement in performance when compared to single-phase microchannel devices, suggesting that as our understanding of phase change in microchannels improves we can expect a further improvement in the performance of microchannel heat exchangers. Mass transfer is similar to heat transfer in microchannels. The residence time that reactants need to reach complete conversion in a catalytic gas phase reactor also decrease by D^2 if the residence time is dominated by diffusion rather then reaction kinetics. Many important reactions such as steam reforming are catalytic gas phase reactions where the primary barrier to short residence time is the time it takes for the reactant to diffuse to the catalyst site and for the products to diffuse back into the bulk flow. Reductions in residence time and reactor size on the order of a factor of 20 have been reported in the literature. Ultimately, by going to smaller channels we will reduce the diffusion barrier to the point where reaction kinetics will determine residence time for complete chemical conversion.

14.2.2 Applications of MECS Technology

The combination of size reductions and improved process control associated with MECS and the promise of high volume mass production (using microlamination)

means that small modular energy and chemical systems will be available at a reasonable cost. The availability of compact and modular energy and chemical systems means that MECS can be applied to both portable and distributed applications.

For heat transfer applications, example technologies include compact, high performance heat exchangers for thermal management and waste heat recuperation. Microscale combustion systems have been developed which take advantage of microchannel heat transfer to produce extremely compact high flux combustion systems. This technology can be used within compact heating and cooling schemes or for compact power generation or propulsion. Mechanically-constrained ultra thin film gas absorption and desorption has been used to reduce the size of absorption-cycle heat pumps and gas absorbers by a factor of 5 to 10. The application of compact heat pumps to microelectronics cooling could significantly reduce heat dissipation needs (Kawano et al. 1998; Little 1990). It is estimated that distributed, compact industrial heat pumps could improve building heating and cooling costs by 25% by eliminating ducting and heat pump cycling losses. Compact heat-actuated heat pumps could provide cooling for an automobile while using exhaust heat as the main energy source. Efforts are currently being made to adapt these systems to man-portable cooling for chemical and biological warfare suits. Targets are to eliminate the need for batteries weighing less than a third of a conventional system.

For chemical reactions where reaction rates are limited by diffusion, microreaction technology has been demonstrated within hydrocarbon fuel processing systems for fuel cells and proposed for distributed environmental clean-up systems and distributed point-of-use chemical synthesis. Hydrogen production systems for automotive fuel cells can reduce the size of automotive fuel reformers by a factor of 10. Integrated fuel cells and fuel reformers will lead to high energy density battery replacements (Benson and Ponton 1993). It is estimated that these types of systems could provide a person with 10 We for one week in a system weighing less than 1 kg. It is also expected that microscale fuel cells and thermoelectric generators capable of generating 50 to 100 milliwatts of power for up to one year are possible with a weight that is between one third and one tenth of the weight of an electrochemical battery system.

MECS microreactor technologies provide opportunities for distributed environmental restoration, in-situ resource processing and CO_2 remediation and sequestration. Examples of environmental restoration applications include catalytic reactor systems for the distributed destruction of PCBs and the in-situ cleanup or neutralisation of contaminated aquifers (Koeneman et al. 1997). MECS-based high flux carbon dioxide absorption units and chemical processing systems could be used for the production of rocket fuel on the moon and on Mars greatly reducing the payload and cost of manned space flight. High flux carbon dioxide absorption units could be used for the removal and sequestration of carbon dioxide from power plant exhaust. Finally, the application of MECS microrection technology to the distributed production of nanoparticles and designer molecules could avert health risks and safety concerns surrounding the distribution of nanotechnology for consumption. Microchannel technology can also facilitate the

miniaturisation of biologically-based processing systems by accelerating the diffusion of cell media, oxygen and other nutrients and by providing excellent temperature control. This technology might be important for high throughput enzymatic reactors and life support systems for tissue-based sensors.

14.3 MECS Fabrication

MECS is a revolutionary technology that has the potential to impact many aspects of how we live. The availability of small, inexpensive but high capacity MECS devices will increasingly make the distributed processing of mass and energy a reality. However, to realise this vision, we must be able to economically and reliably fabricate large numbers of MECS devices.

14.3.1 Challenges

While MECS devices do include geometries with microscale dimensions, the development of the technology has emphasised materials and fabrication techniques that are significantly different from conventional silicon-based micromachining (Paul and Peterson 1999; Martin et al. 1999). Key differences include materials, operating conditions, system sizes and feature sizes. Silicon is not a good material for most MECS devices. Silicon is brittle and has a high thermal conductivity, which can be a problem for many MECS applications (Peterson 1999). Most MECS devices are fabricated out of metals or polymers with some work being done on the fabrication of ceramic MECS devices. One challenge is to develop fabrication approaches that are appropriate for the many different materials and operating conditions encountered in MECS devices.

Many MECS devices operate at high temperatures with chemically reactive products. Often microreactors will operate at 500 to 600°C and in some applications, designers would like to operate the microreactors at temperatures approaching 1000°C. Suitable fabrication techniques exist for materials that can operate at temperatures up to 600°C but above 600°C difficulties in microlamination of refractory metals and ceramics is a significant challenge. MECS technology will require better methods for fabricating high temperature and chemically inert microscale geometries. Regarding system size, MECS applications will often require arrays of microscale geometries that cover between 1 and 400 cm^2 and this must be at a low cost. Many conventional microfabrication techniques cannot economically process large surface areas. This requires the development of new approaches or a significant improvement in the capabilities of existing microfabrication techniques.

Much of the promise of MECS depends on the availability of a large number of inexpensive distributed components that can compete with the centralised processing of mass and energy. To be competitive, MECS devices must be extremely inexpensive. This will require fabrication techniques that are

appropriate for high volume low cost production with dimensional features across the nano, micro and meso-scales. Traditional prototyping techniques such as diffusion bonding will need to give way to continuous processing techniques such as solder paste bonding and other low cost bonding methods.

14.3.2 Feature Sizes

The most critical dimension in most MECS devices is the height (or width whichever is smaller) of the microchannel though the integration of nano-scale features within microchannels has begun to challenge this assumption. Microchannel dimensions can range from 25 to 250 μm high and 25 μm to tens of mm wide. The sizes of microchannels are determined from a variety of perspectives. From a product design perspective, microchannel heights and lengths impact the residence time of fluid molecules within microchannel reactors or heat exchangers as well as the pressure drop across these devices. In addition, particulate matter within bulk fluids sometimes can present challenges in channel blockage and clogging. For example, consider the separation of hydrogen from gasoline for fuel cell applications. Gasoline contains random particles that can make bulk processing difficult in microchannels with heights below about 100 μm. Further, consider the effect of microchannel size on the overall device shape. MECS devices normally consist of a sequence of unit operations designed either for heat transfer or chemical processing. In order to get bulk fluid flows into the microchannels, a series of headers or plenums are needed each successively decreasing in size. Another way of looking at it is that the headers connect the microchannels to the outside world. Since the major value-added function of MECS devices is carried out in microchannels, generally it is desirable to reduce the volume of header with respect to the volume of microchannel. Due to scaling laws, as the height of microchannels decrease in size, the length of those channels also decrease. Given that the header volume stays relatively the same size, at some point the overall header volume begins to dominate the overall device volume leading to awkward device configurations (e.g. automotive radiators). From a fabrication perspective, as the size of microchannel features decrease, tolerances have more effect on device performance. In other words, a 5 μm error will have more impact on fluid dynamics and heat transfer (due to flow maldistribution) in a 25 μm-high channel than in a 250 μm-high channel. If processing could be performed in a silicon platform, tolerances would permit going well below 5 μm. However, most MECS devices are large compared with IC and MEMS devices and, therefore, bulk material costs are significant. Therefore, monocrystalline silicon is not practical. Further, many MECS devices require thermal or chemical properties not available in silicon architectures. Therefore, many MECS applications need to make use of engineering materials.

The tolerances of many conventional manufacturing processes have been found suitable for microchannels making the economical production of MECS devices more feasible. For example, it has been found that reasonable precision of microchannel heights can be achieved at micro and meso-scale dimensions

through the lamination of shim stock. The advantage of this approach is that the precision tolerances are controlled by an economical, high-volume process such as rolling. In this case, the scale of channel height (the critical feature) is dictated by the thickness of the shim stock, which can normally be sourced down to 25-μm thick. Further, early results showed that the *warpage* produced during the diffusion bonding of copper foils limited microchannel dimensions to no smaller than 80 μm high (Krause et al. 1994) though that constraint has since been lifted.

14.3.3 Microlamination

Current microelectronic integrated circuits (IC) are predominately silicon-based. MECS, on the other hand, require the mechanical and thermal properties provided by other materials. Many thermal applications require low thermal conductivity materials to reduce axial heat transfer (Peterson 1998, 1999). Other requirements for subcomponents could be for highly fatigue resistant material for springs or magnetic steels for generator and motor cores. Many of the prevailing MEMS microfabrication technologies are based on silicon, polymers, or electroplated pure metals (having high thermal conductivity). Adapting these MEMS fabrication techniques for the construction of some MECS devices would be difficult to achieve.

A second requirement for MECS construction is the need for high-aspect-ratio features. Microchannel arrays with >30:1 aspect ratios are commonly needed for heat exchangers and regenerators. Other MECS designs may call for a small gap between adjacent sub-components where the gap is maintained for the entire length of the structure. Other MECS requirements call for heterogeneity in fabrication materials where electrical and magnetic sections may require a metal and dielectric sections may require a polymer or ceramic. Furthermore, electronic circuits may be needed in the overall design of MECS to process information. While MEMS fabrication platforms provide excellent electromechanical integration, these capabilities are limited to planar structures as opposed to three-dimensional, bulk structures.

Finally, MECS must be able to offer all of these capabilities at low cost in order to compete with conventional macro-scale energy and chemical conversion devices. The most notable high-aspect ratio MEMS fabrication technology is LIGA (Becker et al 1986; Ehrfeld et al. 1997). In addition to being primarily a polymer forming method, LIGA is dependent upon highly capital-intensive synchrotron X-ray generation. LIGA and its lower cost derivatives all use lithographic techniques for mold making and electrofoming for mold filling. Weaknesses of this approach include limited material selection, limited geometric complexity (two dimensional structures), and inconsistent pattern-transferring methods (Walsh et al. 1996). Other net-shape microfabrication techniques have been exploited including laser-beam, electron-beam, ion-beam, electrochemical, electrodischarge, and mechanical methods for material removal or deposition. However, all of these approaches are either serial in nature and, therefore, lack the capability of economical mass production, involve single layer thin film forming

and, therefore, provide limited aspect ratios, or are incapable of producing embedded microchannel geometry. No well-established micromechanical fabrication method currently exists for addressing MECS device fabrication requirements in a low-cost, high-volume manner.

For over ten years, Oregon State University and the Pacific Northwest National Laboratory (Richland, Washington) have been developing microlamination techniques for producing high aspect ratio MECS devices. The fabrication methods being pursued by these groups rely on the patterning and bonding of thin layers of material (laminae) to make monolithic assemblies with embedded microchannel circuits (Fig. 14.2). Microlamination is not a process rather, it is a processing architecture. All microlamination techniques involve three steps: 1) lamina patterning; 2) lamina-to-lamina registration to form a stack; and 3) bonding of the stack into a monolith.

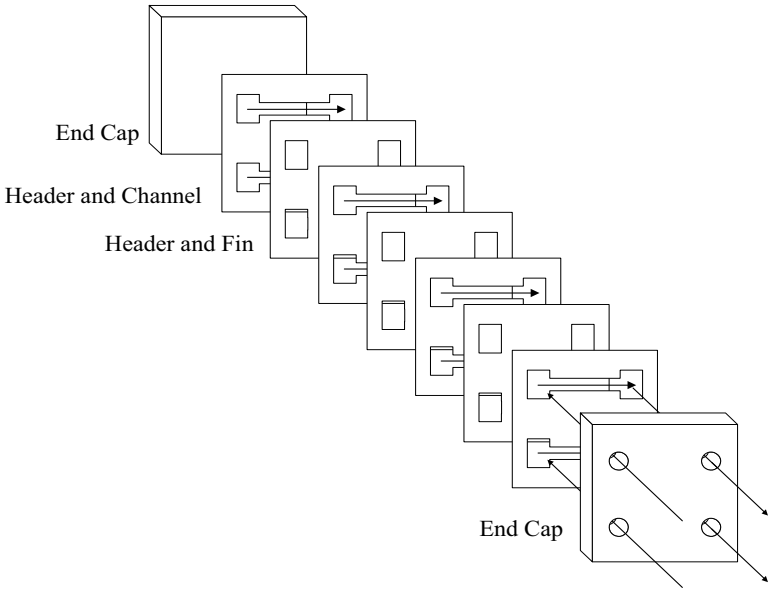

Fig. 14.2. Microlamination scheme used to fabricate a dual micro-channel array. Arrow shows direction of flow

Typical lamina patterning techniques used for metals include photochemical machining, wire electrodischarge machining, electrochemical machining, punching and laser machining (Wegeng and Drost 1994). Photochemical and electrochemical machining have the potential to produce 'blind' features which can be important for reducing the number of laminae per stack or for creating free-standing features such as posts needed to prevent microchannel warpage. Patterning processes for polymers include hot embossing, laser machining, injection molding and punching. In addition to being computer-controlled and, therefore, not requiring expensive, inflexible photomasks, laser machining in

polymers has the added advantage of patterning laminae without leaving a burr. Laser burrs in the laser machining of metals can cause difficulties in bonding laminae. Hot embossing and injection molding both provide the ability to produce blind features. Hot embossing offers the ability to produce thinner laminae, which can be important for reducing device volumes. These molding and forming techniques all require tooling which can be produced using more conventional microfabrication techniques. Variants of these polymer-patterning processes have been studied for patterning green tapes for producing patterned ceramic substrates.

Several registration techniques have been employed in microlamination methods including pin, edge, and self-alignment. The technique used depends on the bonding process chosen. The Thermally-Enhanced Edge Registration (TEER) technique has been demonstrated to be an effective technique for registering laminae during thermal bonding processes (Thomas and Paul 2002, 2003). The TEER technique employs the difference in CTE between the bonding fixture and the laminated material to produce a registration force on the laminae at the bonding temperature. By making the bonding fixture from a material that has a lower CTE than the laminae, a clearance will exist between the fixture and the laminae at room temperature, making the loading of laminae simple compared with other mechanical alignment methods. At the same time, TEER has been shown to achieve a layer-to-layer registration accuracy as small as 2 μm for small microlaminated structures (Thomas and Paul 2002).

Bonding methods that have been explored for metals include diffusion bonding, diffusion brazing, diffusion soldering and solder paste bonding (Kanlayasiri and Paul 2004; Gabriel et al. 2001; Paul et al. 2004). Advantages of diffusion bonding include the ability to work with a homogeneous material. Diffusion brazing and soldering can result in greatly reduced pressure and temperature conditions yielding more robust production methods (less dimensional error). Solder paste-bonding offers the promise of improved economics and the ability to integrate electrical circuits with fluidic circuits. Polymer bonding methods have included solvent welding, thermal bonding, adhesive bonding and ultrasonic welding (Paul et al. 2003). Ultrasonic welding can be easily automated but, along with adhesive bonding, can yield poor channel geometries including particulate matter within microchannels. Solvent welding can leave behind residual solvent which may leach out in subsequent device operation. Thermal bonding can require longer cycle times.

14.4 Dimensional Control in Microlamination

Microlamination has the capacity to fabricate metal, polymer and ceramic devices with high aspect ratios in large production volumes. This has been demonstrated in industry where microlamination has been used to mass produce ink-jet print heads. Development of microlamination methods for production of MECS devices has required research into new lamina patterning processes, bonding techniques, and registration methods.

14.4.1 Effects of Patterning on Microchannel Array Performance

As suggested, microchannel devices are well known for their superior performance in heat and mass transport applications. Much of this is due to the large surface area to volume ratios made possible by the high-aspect-ratio microchannels (HARM) within these devices. In order for these HARM devices to be efficient, pressure drop through these devices must be minimised. Past research has shown that as the channel size decreases within microchannels, the fluid flow behavior within the laminar flow regime of the channel begins to deviate from the traditional Navier-Stokes theory (Pfahler et al. 1990; Rahman and Gui 1993; Zemel et al. 1984). Wu and Little (1983) and Peng et al. (1994) both found that the wall effect in microchannels had a significant impact on the laminar flow behavior within the microchannels. Parameters given for influencing the wall effect included the method used to form microchannel walls. Typically, in metal microlamination, the device is formed from cold-rolled shim stock, which possesses a very smooth surface finish. Therefore, sidewall geometries in metal microlaminated structures are not expected to play a large role in the microfluidic wall effect. A microchannel, however, (Fig. 14.3) formed by microlamination may have significant endwall surface roughness depending upon the method of machining used during the lamina-patterning step. Many techniques have been used for lamina patterning including laser micromachining, photochemical etching, and electrochemical machining. Laser micromachining has been used to form microchannels for microlamination because of its ability to quickly adapt to complex geometry. The endwalls formed by the laser micromachining process are known to be rough. Photochemical etching has been used in microlamination due to its relatively low cost when compared with laser machining.

Matson et al. (1997) suggested the use of photochemical etching to pattern highly complex stainless steel shims to fabricate laminated microchannel chemical reactors with a relatively low cost per shim (less than US$1). However, in photochemical etching processes, the costs of waste treatment and disposal can be greater than the processing costs (Datta and Harris 1997). An alternative process with fewer waste disposal problems is electrochemical micromachining (EMM). EMM is a well-established technique that has been used in the electronics industry to machine thick and thin films. This method is known to provide a very smooth endwall surface. It is expected that for microlaminated channels there exists an aspect ratio limit at which the method of lamina patterning no longer significantly influences the microchannel pressure drop. Knowledge of this limit would be beneficial for device designers of cross-flow and counter-flow microchannel devices where maximum aspect ratio limits are known to exist. Efforts to quantify the end wall effect in microlamination have been reported in Paul et al. (1999). In this study, stainless steel microchannels with various aspect ratios were fabricated with machining techniques resulting in both good (EMM) and poor (deep UV laser micromachining) surface finish. Pressure drop was then tested across the microchannels. The results were compared to see whether there is a difference in the pressure drop performance of the microchannels due to these two machining methods and at what aspect ratio the difference becomes insignificant.

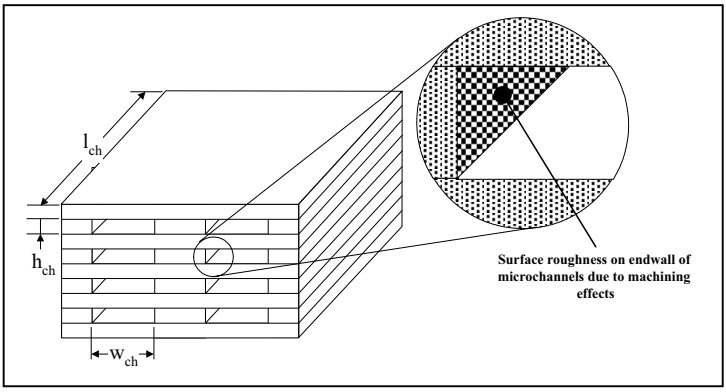

Fig. 14.3. Schematic defining terms associated with a microlaminated geometry

14.4.2 Theory

For fluid flow in a channel, it is well known that the friction factor is not only a function of Reynolds number, but it also depends on the shape of the channel cross section. With the same flow area, the friction factors are different if the channel cross sections are different. Surface roughness of the channel is another important factor for flow in the microchannels because of large relative roughness although the effect is negligible in macro scale fluid (Wu and Little 1983; White 1994). In this experiment, two different shapes of the channel cross-section were considered--rectangular and trapezoid. The difference in the shapes of cross section is caused by different machining methods used in the experiment. The EMM process provides a trapezoidal cross section with smooth end walls whereas laser machining gives a rectangular cross section with rougher end walls. In this study, the range of the volumetric flow rate Q for the microchannel test was set and the pressure drop Δp across the test module was measured. The test module was assumed to have a specific cross-sectional area A and a channel length L. The results are presented in form as a friction factor f and hydraulic diameter D_h. The friction factor is defined as:

$$f = \left(\frac{2\Delta p A^2}{\rho L Q^2} \right) D_h \tag{14.1}$$

Where, ρ is the density of liquid and the hydraulic diameter D_h can be calculated from:

$$D_h = \frac{4 \cdot A}{WettedPerimeter} \tag{14.2}$$

For laser micromachining, the cross-section area is rectangular, so the hydraulic diameter is equal to D_h=2WH/(W+H), where W and H are the channel width and channel height, respectively. On the other hand, the EMM process produces a trapezoidal cross-section. We can calculate the hydraulic diameter in Eq.14.2 by substituting the cross-sectional area and the wetted perimeter of this trapezoidal structure. The cross-sectional area of this structure is equal to the average of the top width *a* and bottom width *b* of the channel multiplied by the channel height *H*, or $A = (a+b)H/2$, where the wetted perimeter will equal to a+b+2{H^2+(1/4(a-b)^2}$^{-1/2}$. The Reynolds number, *Re*, can be calculated from

$$Re = \frac{QD_h}{A\nu} \tag{14.3}$$

Where, ν is the dynamic viscosity of the liquid. As stated in the Moody chart for the laminar flow regime, the relationship of the friction factor in laminar flow, and the Reynolds number is linear, $f = C_f/Re$, where C_f is the friction coefficient for the system. In this study, a simple analysis of the effect of the surface roughness generated by different fabrication techniques on friction coefficients within single channel devices was investigated.

14.4.3 Microchannel Fabrication

Simple single channel devices (Fig. 14.4) were laminated in 304 stainless steel for performing the analysis. The bottom end plate and top interconnect layer were machined from 3 mm thick sheet stock. One batch of the middle stainless steel laminae was machined by one-sided through-mask EMM. The important parts of the patterns were 3 mm diameter sumps and the microchannel. Channel widths and depths explored are shown in Table 14.2. These dimensions were verified by metallography after fabrication and testing of the microchannels. The EMM laminae were set to be machined in the transpassive regime of the electrochemical system to provide a smooth finish. The laser micromached laminae were patterned using a Nd:YAG laser (266 nm) with an average power of 300 mW, an effective spot size of 35 μm and a frequency of 4.5 kHz. Each machined lamina was then diffusion bonded between the two thick end caps with mirror-like finishes (R_a = 0.2 μm). Both end caps were polished to provide extremely smooth surfaces for the bonded microchannel to minimise the effect of sidewall friction. Details of the fabrication procedures are given elsewhere (Wattanutchariya et al. 2003).

The bonded microchannels were pressure drop tested at various flow rates in the laminar flow regime. According to Wu and Little (1983) and Peng et al. (1994) the transition zone from laminar flow to turbulent flow in microchannels occurs much earlier than conventional values. They reported that for different test devices with hydraulic diameters ranging from 0.1 to 0.3 mm, the transition zone varies from Reynolds numbers of 200 to 900. In this study, the maximum Reynolds number was kept to no more than 200, which was still in the laminar flow regime.

Table 14.2. Dimensions and theoretical friction coefficients of experimental channels. Theoretical friction coefficients are from Shah and London (Shah and London 1978)

Channel No.	Machining Method	Top Width (μm)	Bottom Width (μm)	Depth (μm)	Length (μm)	Hydraulic Diameter (μm)	Theoretical C_f
1	Laser	225.4	225.4	78.2	12000	116.1	67.7
2	Laser	319.3	319.3	77.2	12000	124.3	73.5
3	Laser	474.1	474.1	72.3	12000	125.5	80.0
4	Laser	563.8	563.8	74.3	12000	131.2	81.7
5	Laser	678.4	678.4	74.3	12000	133.9	83.8
6	Laser	1037	1037	77.2	12000	143.4	87.3
7	EMM	277.2	162.8	76.2	12000	106.3	62.8
8	EMM	372.2	306.8	74.3	12000	119.9	72.0
9	EMM	507.7	454.2	74.3	12000	127.6	80.0
10	EMM	591.3	510.5	75.3	12000	130.3	76.0
11	EMM	656.2	656.2	78.2	12000	139.7	82.9
12	EMM	1296.3	1111.1	73.4	12000	133.7	84.0

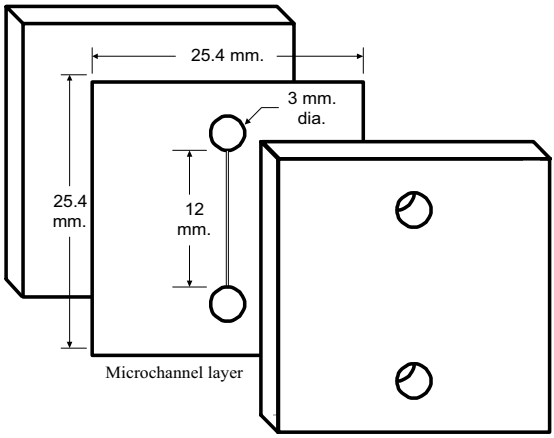

Fig. 14.4. Schematic of a microchannel layer and end caps

14.4.4 Results

To obtain the microchannel dimensions, metallography was performed on the test devices. Fig. 14.5 and Fig. 14.6 represents the cross-section views of the diffusion bonded test devices of channel number 3 and 9, which were fabricated by laser micromachining and by electrochemical micromachining respectively. Fig. 14.7 shows a comparison of the theoretical and experimental friction coefficients for

the set of microchannels from which the channels in Fig. 14.6 came. A summary comparison of the theoretical and experimental friction coefficients are shown in Fig. 14.8 as a function of aspect ratio.

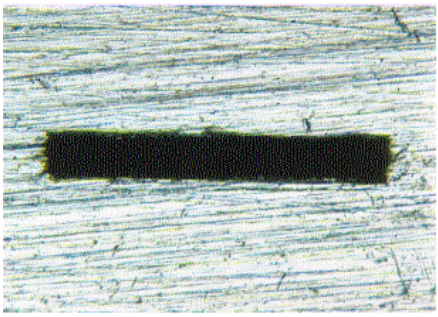

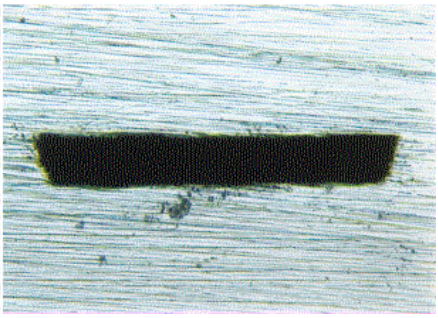

Fig. 14.5. Laser Micromachining; **Fig. 14.6.** EMM

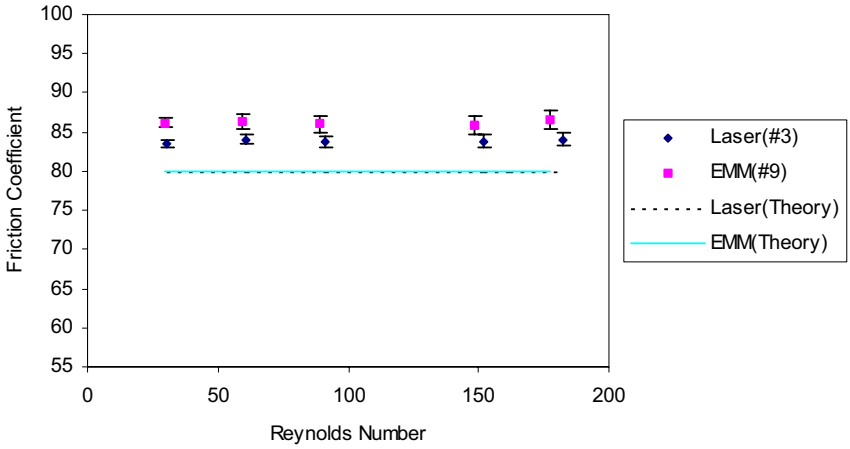

Fig. 14.7. Friction coefficient as a function of Reynold's number for channels 3 (aspect ratio 7:1) and 9 (aspect ratio 6:1). The theoretical friction coefficients happen to coincide for these two channels

From the results, the friction coefficients of both laser-machined channels and electrochemically-machined channels were found greater than the corresponding theoretical values and the differences from theory are significantly greater for laser-machined channels. In Fig. 14.8, at 2:1 aspect ratio, the friction coefficient of the laser-machined microchannel differs by about 40% from that of the electrochemically-machined microchannel. As the aspect ratio of the microchannels increases, the difference in friction coefficient decreases generally and when the aspect ratio reaches 9:1, the value of friction coefficient becomes almost the same. This provides some evidence that the machining method does

play a significant role in MECS device performance at lower aspect ratios. Lower aspect ratio features produced by methods yielding higher surface roughnesses will result in increased flow friction causing the need for greater pumping powers. Based on this analysis, it would seem that this impact on fluid flow behavior in microchannels is directly related to the end wall surface roughness of the microlaminated microchannels. Further, this particular study indicates that the effect of the machining method in microlamination is no longer significant if the aspect ratio of the microchannel is greater than about 9:1.

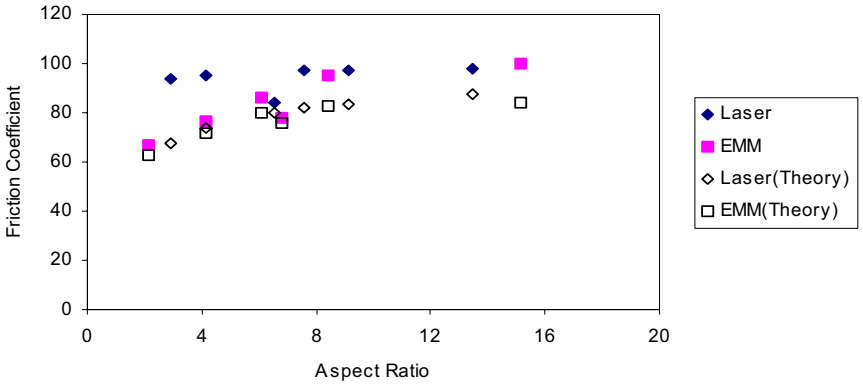

Fig. 14.8. Average friction coefficient and aspect ratios of the microchannels

It is also interesting to note that the difference between the theoretical and experimental values for the friction coefficient in the electrochemically-machined channels is minimal below an aspect ratio of about 8:1 but then increases significantly beyond this point. This phenomenon can be explained by noting that at low aspect ratios, where the end walls have strong influence, the surface roughness of end walls dominates pressure drop across the channel. Since EMM is known to produce perhaps the best surface finish of all non-traditional machining processes, the good agreement between the experiment and theory in those channels at low aspect ratio is not surprising. The deviation from theoretical friction coefficient at higher aspect ratio is explained in Fig. 14.9. Investigation of the higher aspect ratio channels showed a slight deflection in the sidewalls of these channels resulting in a decrease in the cross-section of the channels. This suggests that at aspect ratios above 10:1, sidewall deflection appears a more dominant constraint to aspect ratio than machining method. It is interesting that this type of shape variation appeared even though the thickness of the sidewall end plates was increased significantly to circumvent this problem. It is anticipated that this type of fin warpage behavior will become more pronounced at higher aspect ratios especially inside of spatially-intensified MECS devices where fin thicknesses will be more on the order of microchannel heights. Therefore, the effect of patterning methods on end wall surface roughness should be considered in the design and fabrication of microlaminated MECS devices with low aspect ratio features.

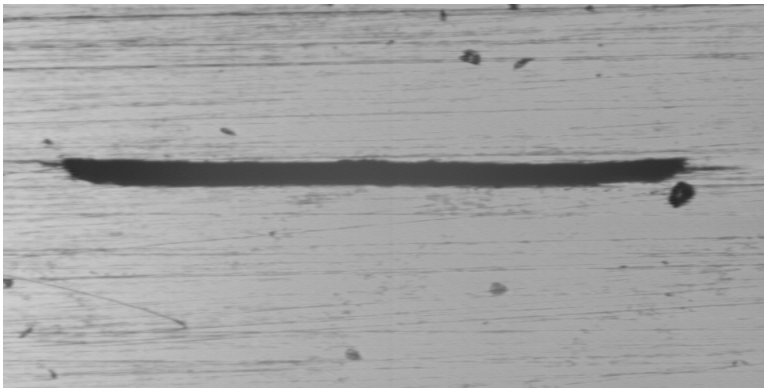

Fig. 14.9. Cross section of channel number 12

14.5 Sources of Warpage in Microchannel Arrays

Several sources have been identified for causing warpage within microchannel arrays. As shown above, one source of microchannel warpage can be the application of bonding pressure on regions of external laminae adjacent to microchannel regions. Another noted source of warpage can come directly from warpage in the raw shimstock, foil or film. Out of the box, even annealed, cold-rolled shimstock can have flatnesses greater than 50 μm on a 50 μm thick foil (Wattanutchariya and Paul 2004). Consequently, flattening procedures are generally required for precision microchannel array fabrication prior to the patterning step. Unannealed metal foils are particularly susceptible to warpage during the bonding cycle due to the relaxation of residual stresses built up in the foils during cold rolling or electrodeposition (in the case of electroplated foils). Perhaps the greatest source of warpage can come from sideloads on the foils either due to friction between laminae, friction between external laminae and the fixture or due to the registration technique. Slower temperature ramps in the bonding cycles can help to ameliorate some of these causes of warpage. Also, application of bonding pressure at the bonding temperature is a must to avoid sideloads caused by friction. Pin registration is particularly troublesome in thermal bonding processes if the coefficient of thermal expansion between the fixture and the laminae are different. As an example, the following analysis explains the effect that the TEER technique can have on fin buckling and registration behavior. Fig. 14.10 illustrates a simple TEER setup. Several laminae are aligned to one another with the use of a TEER fixture. The distance between the posts in the TEER fixture is referred to as the fixture slot width (W_s). At any temperature, the allowance (A) between the width (W) of the laminae and W_s is:

$$A(T) = W(T) - W_s(T) = W \cdot (1 + \alpha_{ss} \Delta T) - W_s \cdot (1 + \alpha_g \Delta T) \qquad (14.4)$$

Where, A is the allowance between the fixture and the laminae which are both a function of temperature (T), α_{ss} is the CTE of stainless steel, α_g is the CTE of graphite and ΔT is the change in temperature from room temperature.

When applying the TEER technique during a diffusion bonding cycle, the metal laminae and the bonding fixture are heated up to a specific temperature, normally in the range of about 60% to 75% of the melting temperature of the base material. For diffusion bonding of metallic structures, this temperature can be 1000 °C or higher. Within a TEER procedure, the fixture and laminae will expand differently as the temperature is raised resulting in a registration force on the laminae at the bonding temperature. However, if this registration force is higher than the critical buckling load of the microchannel fin, buckling of the fin will occur. This is illustrated in Fig. 14.11. When buckling develops, flow channels that are separated by the buckled fin are no longer uniform resulting in flow maldistribution and a drop in the effectiveness of the microchannel array. Fig. 14.12 shows nonuniform microchannels produced as a result of fin buckling. Fig. 14.13 illustrates the result from a previous investigation conducted by Thomas of the TEER technique for microlamination. The graph shows the relationship between the allowance of the bonding fixture and laminae versus the amount of misalignment. This picture suggests that there is an interval of allowance between the laminae and the bonding fixture, where the misalignment is somewhat constant. From this graph, it is observed that once interference is established the accuracy of registration is not improved further. On the other hand, if this interference extends beyond a certain point, the fin will buckle. This indicates that interference should remain within a particular range. This range should constrain the allowable tolerance of the fixture, governed by the desired registration accuracy and the buckling of the laminae.

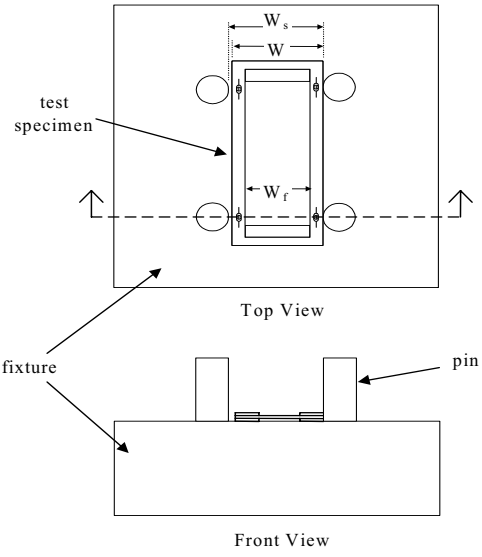

Fig. 14.10. Loading of laminae into a TEER fixture

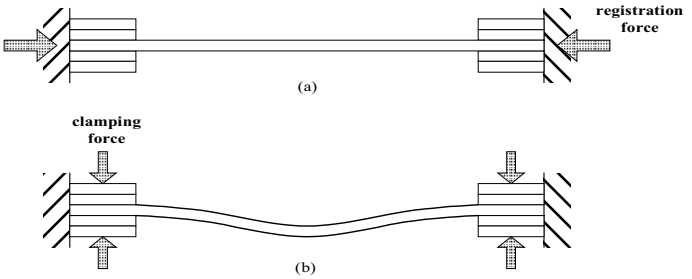

Fig. 14.11. Schematic of fin buckling due to excess registration force

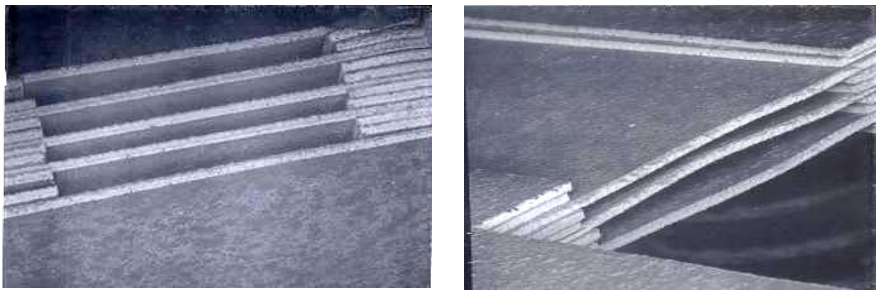

Fig. 14.12. SEM micrographs of a microchannel heat exchanger with nonuniform flow channels (a) before and (b) after fin buckling (Courtesy: Albany Research Center)

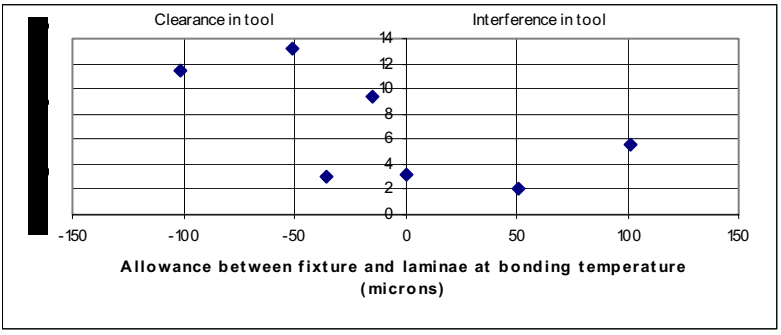

Fig. 14.13. Graph of misalignment versus allowance between fixture and laminae at bonding temperature

14.5.1 Analysis

Assumptions for the following derivation are reported. At some critical temperature called the registration temperature (T_r), the allowance between the

fixture and the laminae will be zero. Under these conditions, W can be solved for in terms of W_s:

$$W = \frac{W_s \cdot (1 + \alpha_g \Delta T_r)}{(1 + \alpha_{ss} \Delta T_r)} \tag{14.5}$$

Where, ΔT_r is the difference between the registration temperature and room temperature. By definition, ΔT_r is defined as:

$$\Delta T_r = \Delta T_{tot} - \Delta T_n \tag{14.6}$$

Where, ΔT_{tot} is the total change in temperature from room temperature to the bonding temperature and ΔT_n is the temperature increase beyond the registration temperature at which interference between the laminae and the fixture occurs (i.e., the bonding temperature is above the registration temperature in order to produce a registration load). To determine if a fin will buckle, the mode of failure needs to be confirmed by calculating several loads. For the fixed-ended boundary condition shown in Fig. 14.11, the critical buckling load (P_c) can be calculated from:

$$P_c = \frac{4 \cdot \pi^2 \cdot E \cdot I}{W_s^2} \tag{14.7}$$

Where, E is Young's Modulus and I is the moment of inertia of the specimen. The second load to be considered is the yield load (P_y) defined as the load necessary to yield the fin in compression which is the product of the yield strength and the cross sectional area of the fin:

$$P_y = \sigma_p \cdot A_f \tag{14.8}$$

The final load to be considered is called the registration load (P_r) due to thermal expansion which occurs beyond the registration temperature. The registration load can be calculated from:

$$P_r = A_f \cdot E \cdot (\alpha_{ss} - \alpha_g) \cdot \Delta T_n \tag{14.9}$$

Beyond the registration temperature, the allowance in Eq.19.4 becomes an interference. To help relate the different load parameters, Fig. 14.14 shows the resultant interference limits at which fin buckling will begin as a function of the fin stiffness and thickness for a typical MECS device configuration (Wattanutchariya and Paul 2004). The shape of this plot shows that the load to plastically compress the material is larger than the critical buckling load up to a

stiffness of about 2.0 x 10^7 kg/s^2 (i.e., thickness of 0.11 mm). Below this stiffness, the fin may buckle elastically if the registration force is less than the yield force. In this case, ΔT_n can be found by substituting the expression for P_y in Eq.19.8 for P_r in Eq.19.9 and solving for ΔT_n:

$$\Delta T_n = \frac{\sigma_p}{E \cdot (\alpha_{ss} - \alpha_g)} \tag{14.10}$$

However, above this stiffness, the fin may yield in compression without buckling if the registration load is larger than the yield load but below the critical load for fin buckling (Gere and Timoshenko 1997). In this case, ΔT_n can be found by substituting P_c in Eq.14.4 for P_r in Eq.14.6 and solving for ΔT_n:

$$\Delta T_n = \frac{P_c}{A_f \cdot E \cdot (\alpha_{ss} - \alpha_g)} \tag{14.11}$$

In either case, if the registration load exceeds both the critical load for fin buckling and the yield load, the fin will permanently buckle. Fig. 14.14 can be used to evaluate the tolerance limits of a bonding fixture to avoid fin buckling for different stiffness of fin layers. This relation also shows that as a fin layer becomes stiffer, buckling becomes less likely in the device because the interference limit in the stiffer fin is allowed to be greater. The magnitude of fin buckling as a function of interference has been derived.

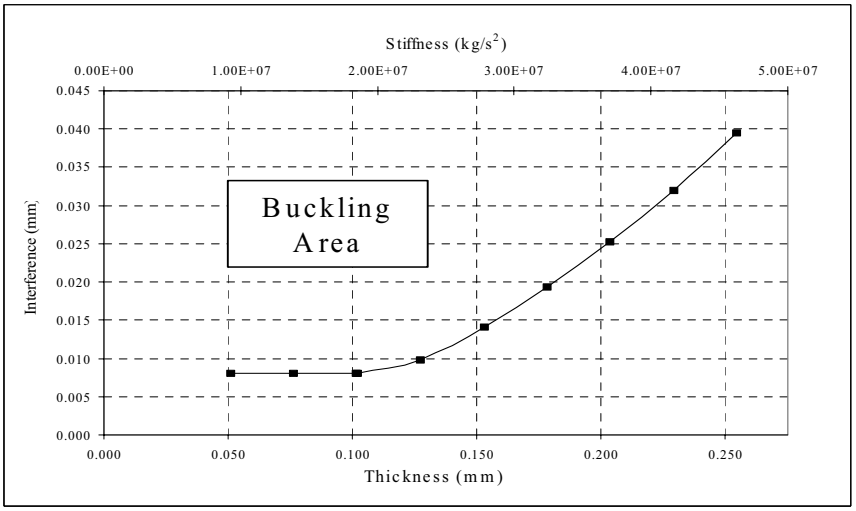

Fig. 14.14. Relationship between fin stiffness or thickness and the allowable fin-fixture interference at the critical point of buckling (Wattanutchariya and Paul 2004)

14.5.2 Results

Fig. 14.15 illustrates both the theoretical and experimental magnitude of maximum buckling deflection with respect to the fixture allowance at the diffusion temperature. Fin width and length were 8.8 and 20 mm respectively and fin thickness varied at 50.8, 76.2 and 101.6 μm. As can be seen from the graph, buckling begins for all three fin thickness at 10 μm of interference. The standard deviation of the channel-to-channel misalignment in interference was about 3.56 μm. This suggests that a fixture with a tolerance of ± 5 μm could on average yield a registration better than the tolerance of the fixture. There was no statistical evidence that the magnitude of warpage depends on the thickness of the shim under the scope of this experiment. In this case, the load at the proportional limit was found to be greater than the critical point of buckling; therefore, all specimens in this experiment were expected to have the same buckling behavior. The significance of this fact is that as the thickness of laminae continues to decrease, the fixture tolerances will not need to continue to decrease below this lower limit. This could be significant as the drive to decrease device dimensions continues.

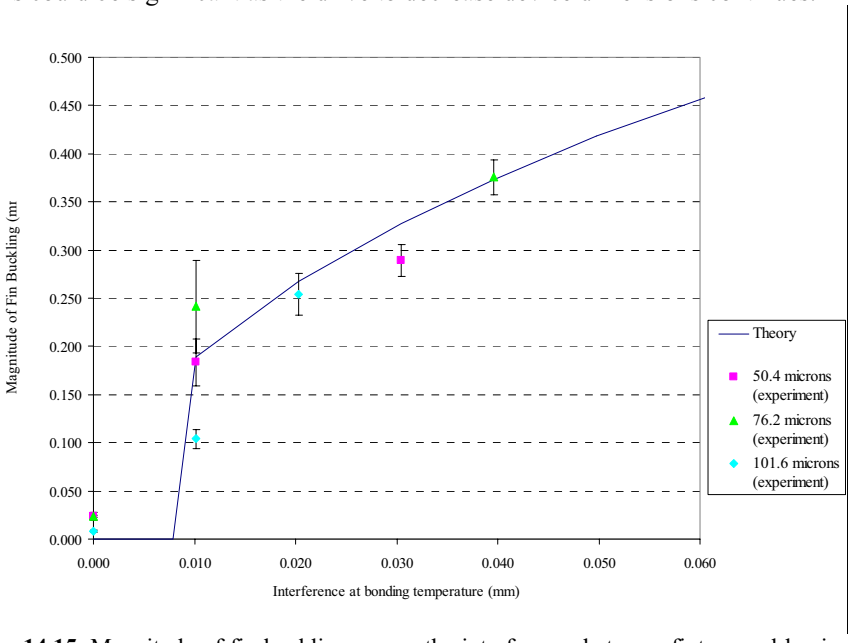

Fig. 14.15. Magnitude of fin buckling versus the interference between fixture and laminae at bonding temperature with 95% confidence interval of standard deviation

As an attempt to increase the tolerance limits of TEER fixtures, an investigation was performed to incorporate compliant mechanisms within TEER fixtures in an effort to increase the allowable tolerance of TEER fixtures (Wattanutchariya and Paul 2004). It was found that for 100 μm laminae, fixture tolerances can be increased from 10 μm to over 100 μm with the use of compliant fixture pins

showing that it is possible to engineer TEER fixtures in a way to bring the fixture tolerances within conventional machining tolerances. These tolerance limits make the fabrication of compliant TEER tools more economical. This compliant TEER technique maintained sub-five μm layer-to-layer registration of buckle-free laminae.

14.6 Effects of Registration and Bonding on Microchannel Array Performance

Several previous investigations have found that the registration step is critical in microlamination. Wangwatcharakul (2002) found that laminae misregistration on the order of 20 μm can cause malfunction of out-of-plane microvalves on the order of 100 μm in diameter. Ashley reported that layer-to-layer bearing gaps on the order of 10 μm were necessary in order to operate the microscale turbine generator developed at MIT (Lohner et al. 1999). In each of these applications, precision alignment of laminae was necessary in order to produce a functional device. However, the effect of misregistration on microchannel array heat exchanger performance has been found to be negligible (Wattanutchariya 2002) though Paul, et al. (2000) found that poor registration in intermetallic microchannel devices resulted in an amplification in the fin warpage found within the device.

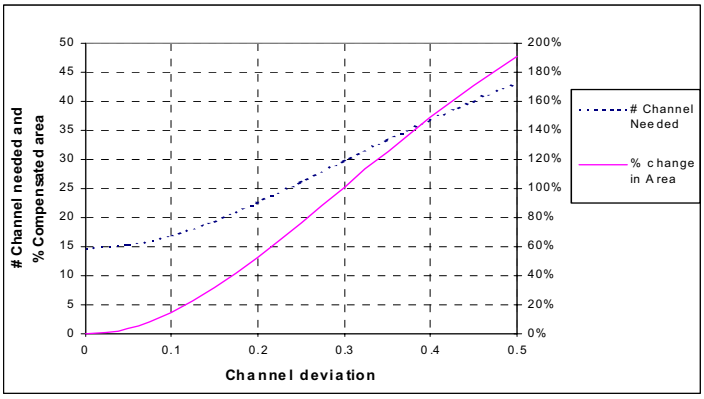

Fig. 14.16. The relation of channel deviation and the number of channel needed as well as percent increase in area to compensate the loss in heat transfer performance

As suggested, the major technological concern in bonding MECS devices is to eliminate fin warpage. Because of the difference in the cross-section of flow channels due to fin warpage, the working fluid will normally flow at different rates between channels. More fluid tends to flow in the larger cross-sectional channels resulting in flow maldistribution. This flow maldistribution results in a

longer diffusion path for heat transfer to or from the wall, resulting in a less effective heat transfer coefficient for the total surface area as well as the overall heat transfer. Wattanutchariya performed an analysis of the effect of flow maldistribution on microchannel heat exchanger performance. Fig. 14.16 illustrates the results of this analysis indicating the percent change in area and change in the total number of microchannels needed to compensate for an average percent channel deviation between adjacent channels within the heat exchanger. Here, percent channel deviation indicates the percent change in channel cross-section as a result of warpage. Fig. 14.16 shows that for a 20% channel deviation, the percent increase in the total number of channels, and, consequently, the heat transfer surface, would need to be 50% to compensate for the loss in heat exchanger performance caused by this deviation. This suggests that channel deviations on the order of 20% of the channel dimension can result in an increase in size of almost 50%.

14.7 Geometrical Constraints in Microchannel Arrays

In the case of heat transfer, the function of a typical microchannel heat exchanger is to transmit the heat from one fluid stream into a second fluid stream. Several different microchannel configurations can be used to accomplish this task. The most efficient heat transfer methods tend to interleave the two fluids in an alternating succession of cross-flow or counter-flow channels. In particular, counter-flow channels are known to provide better temperature distributions along the length of heat exchangers when compared to co-flow heat exchangers (Kakac and Liu 1997). Most MECS applications make use of counterflow microchannel arrays such as in Fig. 14.17. Whereas in the case of co-flow arrays relatively high aspect ratios have been successfully fabricated even in hard-to-produce materials, the aspect ratio is generally constrained in two-fluid microscale heat exchangers because of the more complex geometry.

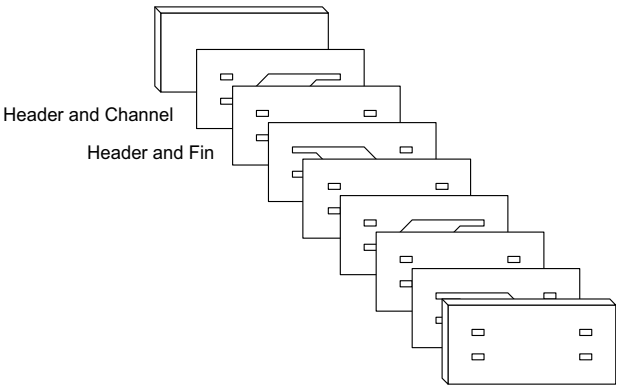

Fig. 14.17. An exploded view illustrating a microlamination procedure

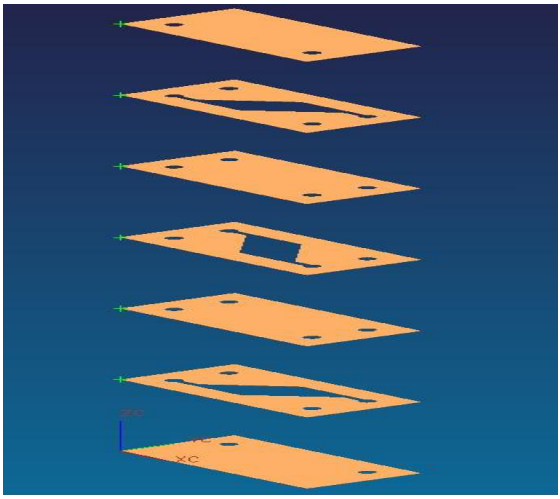

Fig. 14.18. An exploded view of the two-fluid counterflow microchannel array investigated in this study (Model courtesy of P. Kwon at Michigan State University)

The prototypical counter-flow array is produced by alternating layers of microchannels, which allow the two fluids to flow in opposite directions separated by fins. A concept of the through-cut lamina design for a microlaminated counter-flow microchannel array is shown in Fig. 14.18. It is assumed that once the laminae are stacked they are diffusion bonded according to Fig. 14.18. The plan view of the resulting monolith comprised of microchannels and fins is shown in Fig. 14.19. In order to diffusion bond the laminae, a uniform bonding pressure is applied on the stack at an elevated temperature. The pressure is transmitted uniformly through the device except at the necked of the microchannels where each individual microchannel interfaces with fluid headers (the gray regions where the cross-section AA is in Fig. 14.19. The lack of transmitted bonding pressure in these regions can cause the laminae to remain unbonded. In many cases, unbonded regions are observed in the cross-section of counterflow microchannel arrays at points A & B shown in Fig. 14.20, resulting in leakage within the device and mixing of the two fluids.

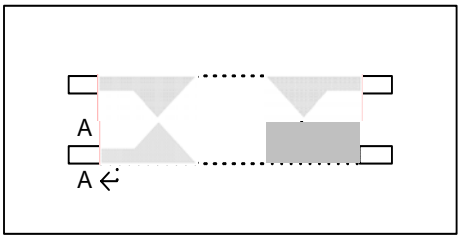

Fig. 14.19. Top view of a counterflow microchannel array comprised of microchannel and fin laminae. The-regions of the device are highlighted in gray

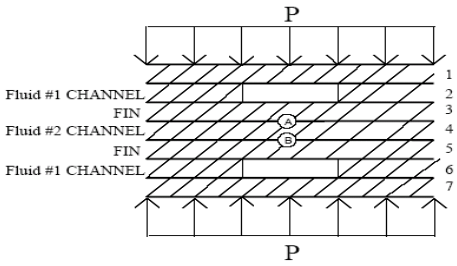

Fig. 14.20. Cross-section of a microchannel neck at cross-section AA in Fig. 14.19. As the width of the channels increase, the stress at points A and B eventually become zero and can even tensile yielding unbounded regions which leak

Fig. 14.21a shows a region within a counterflow microchannel device where pressure was directly transmitted through all of the laminae. Joints between laminae exhibit excellent bonding. Fig. 14.21b shows a region where pressure was not transmitted directly between adjacent laminae because of the counter-flow design. Fig. 14.21b exhibits unbonded regions. From the experience, the width of the necked has to be constrained to a dimension where bonding will occur. The limit on the width of the channel at which bonding takes place depends on the thickness of adjacent fin lamina. In other words, as the thickness of the fin laminae above and below the neck of the microchannels increases, the neck can be made wider. The ratio of the channel span in the necked region to the fin lamina thickness is defined as the fin aspect ratio. The fins in two-fluid microchannel heat exchangers have a certain fin aspect ratio limit beyond which poor bonding will occur within the device resulting in leakage and mixing of the two fluids in the device. Using finite element analysis, it has been found that for a given set of bonding conditions, the key bonding characteristic in all regions of the device must be that only compressive out of plane stresses exist. Maximum fin aspect ratios in the necked regions of counter-flow devices have been implemented up to 10:1 with the allowable fin aspect ratio generally decreasing with increasing fin thickness. This finding is counter-intuitive but has been verified by FEA.

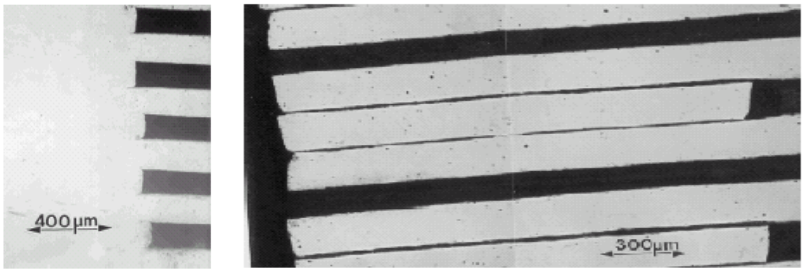

Fig. 14.21. Cross section of a diffusion bounded counter-flow microchannel heat exchanger showing section through which the bonding pressure (a) was transmitted; and (b) was not transmitted. Cross section b resulted in leakage between the two fluids (Micrographs courtesy of Albany Research Center)

14.8 Economics of Microlamination

A key impediment to the proliferation of MECS technology will be its economical production. It is expected that along with the diversity of MECS products that will be developed, there will be a similar diversity with regards to how they are made. Fig. 14.22 shows the unit costs associated with four different microlamination platforms based on photochemical machining (PCM) or blanking/punching (BLK) combined with diffusion bonding (DB) or surface mount technology (SMT). Clearly, the unit cost of MECS devices is better when using blanking/punching and surface mount technology. These improvements are mainly due to decreased cycle times. However, surface mount technology provides the added benefit of reducing the number of laminae needed since the channel laminae are printed using solder paste.

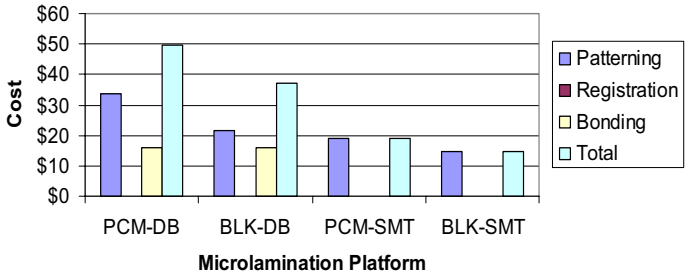

(a)

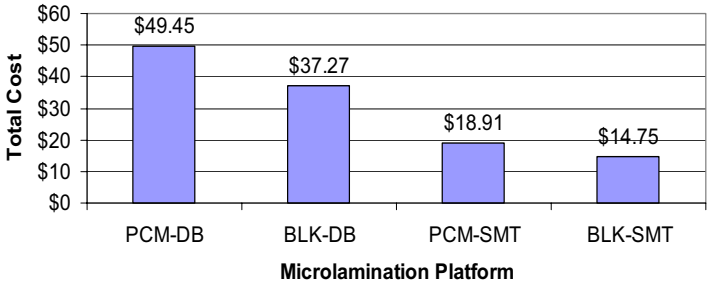

(a)

Fig. 14.22. Unit cost for producing a 50 mm x 50 mm x 100 laminae device at a production rate of 100,000 units/year using four different microlamination platforms: (a) when separated into patterning, registration and bonding costs; (b) estimated unit cost for four different platforms

There are two primary implications of this cost analysis. First, it appears that the cost drivers in microlamination processes are likely to be on the patterning side. This is primarily due to the fact that bonding processes are typically performed only once per device while patterning processes are required for each

individual lamina. Second, a major strategy for reducing costs is therefore to reduce the number of laminae in a particular design (Porter et al. 2002). Consequently, when one thinks of designing MECS devices for cost reduction, the general principle would be to make the device substrates large and few in number. For device configurations that are small, it would make sense to pattern and bond devices in large substrate configurations and die cut individual devices after bonding to distribute patterning and bonding costs across multiple devices. In this sense, the economics of microlamination are similar to those in the IC industry following the trend toward increasingly larger substrate sizes. In a little more than ten years of MECS device fabrication, already device sizes in excess of 70 cm have been proposed compared with IC fabrication where it took more than 40 years to get over 30 cm. The continued development of high production volume processes for fabricating larger and larger device sizes will become increasingly more important.

As suggested, one promising avenue for addressing the economical production of metal MECS devices is the application of SMT (Sharma and Paul 2003). SMT is the practice and method of attaching leaded and non-leaded electrical components to the surface of conductive patterns in the electronic assembly industry. In addition to being an efficient, economical platform for creating solder joints, SMT also provides a platform for integrating electronics into MECS devices. This factor may become more critical as the need to integrate sensors and actuators within MECS devices grows. The bonding process in SMT requires a low temperature of about 300^{o}C and occurs at atmospheric pressure. The reflow process takes 2-3 minutes, which is negligible when compared to techniques like diffusion bonding which takes hours to bond laminae. The printing and reflow processes can be easily automated as well. Finally, the low fabrication temperatures and pressures offered by surface mount technology will help to minimise warpage and residual stress in materials leading to better process control and more sophisticated geometries.

14.9 References

Ameel TA, Papautsky I, Warrington RO, Wegeng RS, Drost MK (2000) Miniaturisation technologies for advanced energy conversion and transfer systems, J. of Propulsion and Power 16:577-582

Ameel TA, Warrington RO, Wegeng RS, Drost MK (1997) Miniaturisation technologies applied to energy systems, Energy Conversion and Management 38:969-982

Ashley S (1997) Turbines on a dime, Mechanical Engineering 119:78-81

Becker EW, Ehrfeld W, Hagmann P, Maner A, Munchmeyer D (1986) Fabrication of microstructures with high aspect ratios and great structural heights by synchrotron radiation, galvanoforming, and plastic molding (LIGA process), Microelectronic Engineering 4:35-56

Beltrami I, Joseph C, Clavel R, Bacher J, Bottinelli S (2004) Micro- and nanoelectric-discharge machining, J. Mat Proc Tech. 49:263-265

Benson RS, Ponton JW (1993) Process miniaturisation: A route to total environmental acceptability?, Trans. IchemE. 71A:160-168

Brooks KP, PM Martin, MK Drost, Call CJ (1999) Mesoscale combustor/evaporator development. Proc. of the ASME, vol. 9, pp 1-50

Brunger WH, Kohlmann KT (1992), E-beam induced fabrication of microstructures. Proc. IEEE microelectromechanical systems, Germany, pp 168-170

Datta M, Romankiw LT (1989) Application of chemical and electrochemical micromachining in the electronics industry, J. Electrochemical Society 136:285-292

Datta M, Harris D (1997) Electrochemical micromachining: An environmentally friendly, high speed processing technology, Electrochimica Acta. 42:3007-3013

Daymo EA, Wiel DP, Fitzgerald SP, Wang Y, Rozmiarek RT, LaMont MJ, Tonkovich ALY (2000) Microchannel fuel porcessing for man portable power. AIChE Spring National Meeting, Atlanta, pp 1-5

Drost MK, Friedrich M (1997) Miniature heat pumps for portable and distributed space conditioning applications, Proc. of IECEC 2:1271-1274

Drost MK, Friedrich M, Martin C, J Martin, Hanna B (1999) Mesoscopic heat-actuated heat pump developmen. Proc. of the ASME vol. 39, New York

Drost MK, Wegeng RS, Martin PM, Brooks KP, Martin JL, Call C (2000) Microheater AIChE National Meeting. Technical Report, AIChE, Atlanta, pp 1-6

Ehrfeld W, Bley P, Gotz F, Hagmann P, Maner A, Mohr A, Moser HO, Munchmeyer D, Schelb W, Schmidt D, Becker EW (1987) Fabrication of microstructures using the LIGA process. Proc. IEEE Micro Robots and Teleoperators Workshop, p 160

Friedrich C, Kikkeri B (1995) Rapid fabrication of molds by mechanical micromilling: process development. Proc. SPIE, vol. 2640, pp 161-171

Gabriel M, Paul BK, Wilson RD, Alman DE (2001) Characterisation of metallic foil joints using diffusion bonding and diffusion soldering in microtechnology-based energy and chemical systems, Transactions of NAMRC XXIX, Gainesville

Gere JM, Timoshenko SP (1997) Mechanics of materials. Boston: PWS-KENT Pub. Co.

Holmes AS, Saidam SM, Lawes RA (1997) Low cost LIGA processes. IEE Microengineering Technologies and How to Exploit Them, IEE digest pp 54-59

Ihlemann J, Schmidt H, Wolff-Rottke B (1993) Excimer laser micromachining, Adv. Materials for Opt. Electr. 2:87-92

Kakac S, Liu H (1997) Heat exchangers-selection, rating, and thermal design. CRC Press, Boca Raton

Kanlayasiri K, Paul BK (2004) A nickel aluminide microchannel array heat exchanger for high-temperature applications, J. Mfg Processes 6:17-25

Kawano K, Minakami K, Iwasaki H, Ishizuka M (1998) Microchannel heat exchanger for cooling electrical equipment. Proc. of the ASME (Heat Transfer Division), vol. 361-3, pp 173-180

Koeneman PB, Busch-Vishniac IJ, Wood KL (1997) Feasibility of micro power supplies for MEMS, J. MicroElectoMechanical Sys. 6:355-362

Krause V, Treusch HG, Loosen P, Kimpel T, Biesenbach J, Kosters A, Robert F, Oestreicher H, Marchiano M, DeOdorico B (1994) Microchannel coolers for high power laser diodes in copper technology. Proc. of the SPIE, vol. 2148

Little WA, (1990) Microminiature refrigerators for Joule-Thomson cooling of electronic chips and devices. Advances in Cryogenic Engineering 35:1325-1333

Lohner KA, Chen KS, Ayon AA, Spearing SM (1999) Microfabricated silicon carbide microengine structures. Proc. of Material Resource Society Symposium, vol. 546, pp. 85-90

Martin PM, Matson DW, Bennett WD, Stewart DC, Lin Y (1999) Laser micromachined and laminated microfluidic components for miniaturised thermal, chemical and biological systems. Proc. of SPIE, vol. 3680, pp 826-833

Martin PM, Matson DW, Bennett WD (1999b) Microfabrication methods for microchannel reactors and separations systems, Chemical Engineering Communications 173:245-254

Martin PM, Matson DW,Bennett WD (1999) Microfabrication Methods for Microchannel Reactors and Separations Systems , Chemical Engineering Communications, 173, 245-254

Matson DW, Martin PM, Bennett WD, Stewart DC, Johnston JW (1997) Laser micromachined microchannel solvent separator. Proc. of Micromachining and Microfabrication Process Technology III, Austin

Matson DW, Martin PM, Stewart DC, Tonkovich ALY, White M, Zilka JL, Roberts GL (1999) Fabrication of microchannel chemical reactors using a metal lamination process. 3rd Int. Conf. on microreaction technology, Frankfurt, pp 1-11

Paul BK, Klimkiewicz M (1996) Application of an environmental scanning electron microscope to micromechanical fabrication, Scanning 18:490-496

Paul, B.K., R.B. Peterson, and W. Wattanutchariya (1999) The effect of shape variation in microlamination on the performance of high-aspect-ratio, metal microchannel arrays, Proc. of the 3rd Int. Conf. on Microreaction Tech., Frankfurt, pp 53-61.

Paul B, Peterson R (1999) Microlamination for microtechnology-based energy, chemical and biological systems. Proc. of the ASME, vol. 39, New York

Paul BK, Dewey T, Alman D, Wilson RD (2000) Intermetallic Microlamination for high-temperature reactors. 4th Int. Conf. nn Microreaction Tech., Atlanta, pp 236-243

Paul BK, Aramphongphun C, Chaplen F, Upson R (2003) An evaluation of packaging architectures for tissue-based microsystems, Transactions of NAMRC XXXI, Hamilton, Canada

Paul BK, Thomas J (2003) Thermally-enhanced edge registration (TEER) for aligning metallic microlaminated devices, J. Mfg Processes 5:185-193

Peng XF, Peterson GP, Wang BX (1994) Frictional flow characteristics of water flowing through rectangular microchannels, Experimental Heat Transfer 7:249-264

Peterson RB (1999) Numerical modeling of conduction effects in microscale counter flow heat exchangers, Microscale Thermophysical Engineering 3:17-30

Peterson RB (1998) Size limits for regenerative heat engines, Microscale Thermophysical Engineering 2:121-131

Peterson RB (2001) Small Package, Mechaninal Engineering

Pfahler J, Harley J, Bau H, (1990) Liquid transport on micron and submicron channels, sensors and Actuators A 23:431-434

Porter JD, Paul BK, Ryuh B (2002) Cost drivers in microlamination based on a high-volume production system design. ASME International Mechanical Engineering Congress and Exposition, New Orleans, Paper no. IMECE2002-32896

Rahman MM, Gui F (1993) Experimental measurements of fluid flow and heat transfer in microchannel cooling passages in a chip substrate, Advances in Electronic Packaging 4:685-692

Sharma N, Porter JD, Paul BK (2003) Understanding cost drivers in microlamination approaches to microsystem development. IIE IERC, Portland, Oregon

Thomas J, Paul BK (2002) Thermally-enhanced edge registration (TEER) for aligning metallic microlaminated devices, Transactions of NAMRC XXX:663-670

Tonkovich AY, Call CJ, Zilka JL (1998) Catalytic partial oxidation of methane in a microchannel chemical reactor, process miniaturisation. 2nd Int. Conf. on Microreaction Technology, American Institute of Chemical Engineers, New York

Toyoda N, Yamada I (2004) Optical thin film formation by oxygen cluster ion beam assisted depositions, Appl. Surf. Science 226:231-236

Tseng A, (2004) Recent developments in micromilling using focused ion beam technology, J. Micromech Microengr 14:15-34

Weigl BH, Yager P (1999) Microfluidic diffusion-based separation and detection, Science 283:346-347

Walsh ST, Boylan R, Warrington R, Elders J (1996) The emerging infrastructure for MEMS based sensor innovation. Proc. Sensors Expo, Anaheim, p 431

Warren et al. (1999) Mesoscale machines and electronics: There's plenty of room in the Middle. Proc. of the ASME, vol. 39, New York

Wangwatcharakul W (2002) Development of a passive micro-ball valve. MS thesis, Oregon State University

Wattanutchariya W, Kannlayasiri K, Paul BK (2003) Effect of machining methods on flow friction behavior in microchannels. Proc. of the 12th IE-Network Conf., Thailand, pp. 125-130

Wattanutchariya W, Paul BK (2004) Bonding fixture tolerances for high-volume metal microlamination based on fin buckling and laminae misalignment behavior, J. Intl Soc Prec. Engr. Nanotechology 28:117-128

Wattanutchariya W, Paul BK (2004) The effect of fixture compliance on thermally-enhanced edge registration in microlamination, accepted in J. Mfg SE

Wegeng RS, Call CJ, Drost MK (1996) Chemical System miniaturisation, AIChE, New Orleans

White FM (1994) Fluid mechanics. 3th edn, McGraw Hill, Singapore

Wu P, Little WA (1983) Measurement of friction factors for the flow of gases in very fine channels used for microminiature Joule-Thomson refrigerators, Cryogenics 273-277

Zemel JN, Harley JC, Pfahler JN, Urbanek W, Bau HH (1994) Fluid transport in microchannels. Proc. of the Symposium on Microstructures and Microfabricated Systems, vol. 94, pp 210-219